Multipath-based SLAM Exploiting AoA and Amplitude Information

Erik Leitinger*, Stefan Grebien*† , and Klaus Witrisal*†

*Graz University of Technology, Graz, Austria ({erik.leitinger,stefan.grebien,witrisal}@tugraz.at)
†Christian Doppler Laboratory for Location-aware Electronic Systems

***Abstract*—In this paper, we present a Bayesian feature-based simultaneous localization and mapping (SLAM) algorithm that exploits multipath components (MPCs) in radio-signals. The proposed belief propagation (BP)-based algorithm enables the estimation of the position, velocity, and orientation of the mobile agent equipped with an antenna array by utilizing the delays and the angle-of-arrivals (AoAs) of the MPCs. The proposed algorithm also exploits the statistics of the complex amplitudes of MPC parameters, i.e. amplitude information (AI), to calculate the detection probabilities of the features. It is therefore suitable for unknown and time-varying detection probabilities. For improved initialization of new virtual anchor (VA) positions, the states of unobserved potential VAs are modeled as a random finite set and propagated in time by means of a "zero-measurement" probability hypothesis density filter. We analyze the proposed BP-AI-based SLAM algorithm using synthetic and real measurements enabling robust localization in a challenging environment.**

I. Introduction

Simultaneous localization and mapping (SLAM) is important in many fields including robotics [1], autonomous driving [2], [3], location-aware communication [4], and robust indoor localization [5], [6]. Specifically, robustness, i.e. achieving a low probability of localization outage, is still a challenging task in environments with strong multipath propagation [7]–[9]. Therefore, new systems supporting multipath channels either take advantage of it by exploiting multipath components (MPCs) for localization [5], [6], [10], exploiting cooperation among agents [11]–[14], and/or exploiting robust signal processing against multipath propagation and clutter measurements in general [15], [16].

In [17], we extended a belief propagation (BP) algorithm for feature-based SLAM [6], [18] to incorporate the statistics of the MPC amplitudes [19]. The algorithm jointly performs probabilistic data association (DA) and sequential Bayesian estimation of the state of a mobile agent and the states of "potential features" (PFs) characterizing the environment [6], [15], [20]. The PFs are augmented by a binary existence variable, associated with a *probability of existence* and with normalized amplitudes which are related to the signal-to-interference-plus-noise-ratios (SINRs). The SINRs are the power ratios of the deterministic MPCs and the interfering AWGN plus dense multipath (DM) and thus a measure of the impact of multipath. With the normalized amplitudes adaptive detection probabilities are calculated [7], [21].

The proposed algorithm enables the estimation of the position, velocity, and orientation of the mobile agent equipped with an antenna array by utilizing the delays, the angle-of-arrivals (AoAs) and the amplitudes of the MPCs. The estimated MPC delays/AoAs are associated with delays/AoAs modeled by the geometric relations between the agent and physical anchors (PAs) or virtual anchors (VAs) [21]; the VAs are mirror images of the PAs, as illustrated in Fig. 1. Associated MPCs thus correspond to PAs or VAs, collectively denoted as "features". As presented in [6], the proposed algorithm distinguishes between legacy PFs, which correspond to features that already generated measurements in the past, and new PFs, which correspond to features that generate measurements for the first time. The parameters required to initialize new PFs are modeled in this work explicitly by means of an undetected feature state and are inferred using a "zero-measurement" probability hypothesis density (PHD) filter, which was introduced in the context of multi-target tracking (MTT) in [20], [22]–[24]. This works extends [6], [17] in the following aspect:

- It extends the likelihood function to the AoA of MPCs, enabling the estimation of the agents' orientation.
- It introduces the "zero-measurement" PHD filter to the algorithm presented in [17] and adapts it to the augmented PF states, containing the normalized amplitudes.

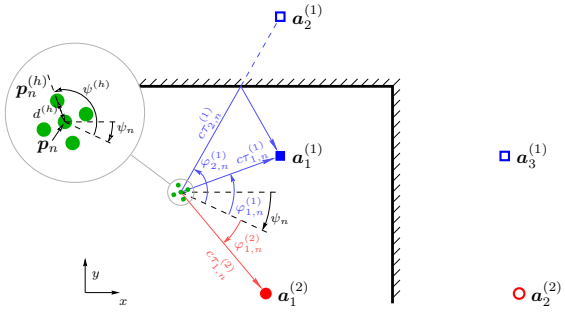

Fig. 1. Exemplary environment in a room corner . The mobile agent at unknown position $\boldsymbol{p}_n$ is equipped with an array, indicated by green dots. The PAs at positions $\boldsymbol{a}_1^{(1)}$ and $\boldsymbol{a}_1^{(2)}$ are marked by a blue box and red bullet, respectively. The red circles and blue squares outside the room indicate some VAs associated with the two PAs.

II. Signal Model

The agent is equipped with an H-element antenna array. At every discrete time step n, the element locations are denoted by $\boldsymbol{p}_n^{(h)}$, $h \in \{1, \ldots, H\}$, the agent position $\boldsymbol{p}_n$ refers to the center of gravity of the array. We also define $d^{(h)} = \|\boldsymbol{p}_n^{(h)} - \boldsymbol{p}_n\|$ and $\psi^{(h)} = \angle(\boldsymbol{p}_n^{(h)} - \boldsymbol{p}_n) - \psi_n$, the distance from the reference location $\boldsymbol{p}_n$ and the orientation, respectively, of the h-th element. The array orientation ψ_n is unknown.

This work was supported in part by the Austrian Science Fund (FWF) under grant J 4027 and by the Christian Doppler Research Association, the Austrian Federal Ministry for Digital and Economics Affairs and the National Foundation for Research, Technology and Development.

At every time n, anchor $j \in \{1,\dots,J\}$ transmits a baseband signal $s(t)$ centered at carrier frequency f_c. The signal at antenna element h is then given as

$$s_{\mathrm{RX},n}^{(j,h)}(t) = \sum_{l=1}^{L_n^{(j)}} \alpha_{l,n}^{(j,h)}\, s\big(t-\tau_{l,n}^{(j,h)}\big) + \nu_n^{(j,h)}(t) + w_n^{(j,h)}(t). \quad (1)$$

The first term on the right-hand side (RHS) describes $L_n^{(j)}$ specular MPCs with complex amplitudes $\alpha_{l,n}^{(j,h)} = \alpha_{l,n}^{(j)} \exp\big(i2\pi f_\mathrm{c} \frac{d^{(h)}}{c} \cos\big(\varphi_{l,n}^{(j)} - \psi_n - \psi^{(h)}\big)\big)$ and delays $\tau_{l,n}^{(j,h)} = \tau_{l,n}^{(j)} - \frac{d^{(h)}}{c}\cos(\varphi_{l,n}^{(j)} - \psi_n - \psi^{(h)})$ with $\tau_{l,n}^{(j)} = \big\|\boldsymbol{p}_n - \boldsymbol{a}_l^{(j)}\big\|/c$ (c as speed of light) and AoA $\varphi_{l,n}^{(j)} = \angle(\boldsymbol{a}_l^{(j)} - \boldsymbol{p}_n) - \psi_n$ related to the distance and angle between the agent's position $\boldsymbol{p}_n \in \mathbb{R}^2$ and the PA/VA positions $\boldsymbol{a}_l^{(j)} \in \mathbb{R}^2$, respectively. The second term on the RHS of (1), $\nu_n^{(j,h)}(t)$, represents the DM, which interferes with the position-related, specular MPCs. The last term on the RHS of (1), $w_n^{(j,h)}(t)$, is AWGN with power spectral density N_0. The square root of the SINR of the l-th MPC, i.e., $u_{l,n}^{(j)} = \sqrt{\mathrm{SINR}_{l,n}^{(j)}}$, is termed normalized amplitude, where $\mathrm{SINR}_{l,n}^{(j)}$ is given according to [21, Eq. (40)].

Channel estimation: A sparse Bayesian multipath channel estimator is used to estimate at each time n and for each PA a set of $M_n^{(j)}$ MPC distances $\hat{d}_{m,n}^{(j)} = c\hat{\tau}_{m,n}^{(j)}$ and AoAs $\hat{\varphi}_{m,n}^{(j)}$ and the corresponding complex amplitudes $\hat{\alpha}_{m,n}^{(j)}$, where $m \in \mathcal{M}_n^{(j)} = \{1,\dots,M_n^{(j)}\}$ [25]. To infer the variances $\hat{\sigma}_{\alpha,m,n}^{(j)2}$ of the amplitudes, we use the antenna array at the agent. The measured normalized amplitude is given as $\hat{u}_{m,n}^{(j)} = |\hat{\alpha}_{m,n}^{(j)}|/\hat{\sigma}_{\alpha,m,n}^{(j)}$. The MPC parameters are combined into the measurement vector $\boldsymbol{z}_n^{(j)} = [\boldsymbol{z}_{1,n}^{(j)\mathrm{T}},\dots,\boldsymbol{z}_{M_n^{(j)},n}^{(j)\mathrm{T}}]^\mathrm{T}$, i.e., $\boldsymbol{z}_{m,n}^{(j)} = [\hat{d}_{m,n}^{(j)}, \hat{\varphi}_{m,n}^{(j)}, \hat{u}_{m,n}^{(j)}]^\mathrm{T}$. The vectors $\boldsymbol{z}_n^{(j)}$ are used as noisy "measurements" by the SLAM algorithm.

III. System Model

The state of the mobile agent at time n is defined as $\boldsymbol{x}_n \triangleq [\boldsymbol{p}_n^\mathrm{T}\ \boldsymbol{v}_n^\mathrm{T}\ \psi_n]^\mathrm{T}$, where $\boldsymbol{v}_n = [v_{l,n}\ v_{r,n}]^\mathrm{T}$ is the agent's velocity with $v_{l,n}$ and $v_{r,n}$ as longitudinal and rotational velocity. We use a near-constant turn model [1, Chapter 5] and assume that the array is rigidly coupled with the movement direction. Note that since we do not use an array at the PA, which would enables also the estimation of the angle-of-departure, we need to utilize a second PA to be able to estimate the orientation in the absolute coordinate system defined by the PAs [8]. For each PA j, there are $K_n^{(j)}$ PFs. Thus, the PFs will be indexed by the tuple (j,k), where $j \in \{1,\dots,J\}$ and $k \in \mathcal{K}_n^{(j)} \triangleq \{1,\dots,K_n^{(j)}\}$. Whereas the number of PAs J is known, the number of PFs $K_n^{(j)}$ is unknown and random. The existence of the (j,k)-th PF as an actual *feature* is indicated by the binary existence variable $r_{k,n}^{(j)} \in \{0,1\}$, where $r_{k,n}^{(j)} = 0$ ($r_{k,n}^{(j)} = 1$) means that the PF does not exist (exists) at time n. The state of PF (j,k) is the PF's position $\boldsymbol{a}_{k,n}^{(j)}$, and the *augmented state* of a PF (j,k) is defined as $\boldsymbol{y}_{k,n}^{(j)} \triangleq \big[\underline{\boldsymbol{y}}_{k,n}^{(j)\mathrm{T}}\ r_{k,n}^{(j)}\big]^\mathrm{T}$ with $\underline{\boldsymbol{y}}_{k,n}^{(j)} = \big[\boldsymbol{a}_{k,n}^{(j)\mathrm{T}}\ u_{k,n}^{(j)}\big]^\mathrm{T}$, which includes the normalized amplitude $u_{k,n}^{(j)}$ [6], [17], [20]. We also define the stacked vectors $\boldsymbol{y}_n^{(j)} \triangleq \big[\boldsymbol{y}_{1,n}^{(j)\mathrm{T}} \cdots \boldsymbol{y}_{K_n^{(j)},n}^{(j)\mathrm{T}}\big]^\mathrm{T}$ and $\boldsymbol{y}_n \triangleq \big[\boldsymbol{y}_n^{(1)\mathrm{T}} \cdots \boldsymbol{y}_n^{(J)\mathrm{T}}\big]^\mathrm{T}$. It will be convenient to formally consider PF states also for the nonexisting PFs (case $r_{k,n}^{(j)} = 0$); however, the values of these states are obviously irrelevant. Therefore, all probability density functions (pdfs) defined for an augmented state, $f\big(\boldsymbol{y}_{k,n}^{(j)}\big) = f\big(\underline{\boldsymbol{y}}_{k,n}^{(j)}, r_{k,n}^{(j)}\big)$, are such that for $r_{k,n}^{(j)} = 0$, $f\big(\underline{\boldsymbol{y}}_{k,n}^{(j)}, 0\big) = f_{k,n}^{(j)} f_\mathrm{D}\big(\underline{\boldsymbol{y}}_{k,n}^{(j)}\big)$, where $f_\mathrm{D}\big(\underline{\boldsymbol{y}}_{k,n}^{(j)}\big)$ is an arbitrary "dummy pdf" and $f_{k,n}^{(j)} \geq 0$ can be interpreted as the probability of nonexistence of the PF [6], [17], [20].

At any time n, each PF is either a *legacy PF*, which was already established in the past, or a *new PF*, which is established for the first time. The augmented states of legacy PFs and new PFs for PA j will be denoted by $\tilde{\boldsymbol{y}}_{k,n}^{(j)} \triangleq \big[\tilde{\boldsymbol{a}}_{k,n}^{(j)\mathrm{T}}\ \tilde{u}_{k,n}^{(j)}\ \tilde{r}_{k,n}^{(j)}\big]^\mathrm{T}$, $k \in \mathcal{K}_{n-1}^{(j)}$ and $\breve{\boldsymbol{y}}_{m,n}^{(j)} \triangleq \big[\breve{\boldsymbol{a}}_{m,n}^{(j)\mathrm{T}}\ \breve{u}_{m,n}^{(j)}\ \breve{r}_{m,n}^{(j)}\big]^\mathrm{T}$, $m \in \mathcal{M}_n^{(j)}$, respectively. Thus, the number of new PFs equals the number of measurements, $M_n^{(j)}$. The set and number of legacy PFs are updated according to $\mathcal{K}_n^{(j)} = \mathcal{K}_{n-1}^{(j)} \cup \mathcal{M}_n^{(j)}$ and $K_n^{(j)} = K_{n-1}^{(j)} + M_n^{(j)}$, where the first relation is understood to include a suitable reindexing of the elements of $\mathcal{M}_n^{(j)}$. (The number of PFs does not actually grow by $M_n^{(j)}$ because the set of PFs is pruned [6].) We also define the following state-related vectors: For the legacy PFs for PA j, $\tilde{\boldsymbol{a}}_n^{(j)} \triangleq \big[\tilde{\boldsymbol{a}}_{1,n}^{(j)\mathrm{T}} \cdots \tilde{\boldsymbol{a}}_{K_{n-1}^{(j)},n}^{(j)\mathrm{T}}\big]^\mathrm{T}$, $\tilde{\boldsymbol{r}}_n^{(j)} \triangleq \big[\tilde{r}_{1,n}^{(j)} \cdots \tilde{r}_{K_{n-1}^{(j)},n}^{(j)}\big]^\mathrm{T}$, and $\tilde{\boldsymbol{y}}_n^{(j)} \triangleq \big[\tilde{\boldsymbol{y}}_{1,n}^{(j)\mathrm{T}} \cdots \tilde{\boldsymbol{y}}_{K_{n-1}^{(j)},n}^{(j)\mathrm{T}}\big]^\mathrm{T}$. For the new PFs for PA j, the vectors $\breve{\boldsymbol{a}}_n^{(j)}$, $\breve{\boldsymbol{r}}_n^{(j)}$, and $\breve{\boldsymbol{y}}_n^{(j)}$ with length $M_n^{(j)}$ are defined similarly. For the combination of legacy PFs and new PFs for PA j, $\boldsymbol{y}_n^{(j)} \triangleq \big[\tilde{\boldsymbol{y}}_n^{(j)\mathrm{T}}\ \breve{\boldsymbol{y}}_n^{(j)\mathrm{T}}\big]^\mathrm{T}$. Note that the vector entries (subvectors) of $\boldsymbol{y}_n^{(j)}$ are given by $\boldsymbol{y}_{k,n}^{(j)}$ for $k \in \mathcal{K}_n^{(j)}$. For all the legacy PFs, $\tilde{\boldsymbol{y}}_n \triangleq \big[\tilde{\boldsymbol{y}}_n^{(1)\mathrm{T}} \cdots \tilde{\boldsymbol{y}}_n^{(J)\mathrm{T}}\big]^\mathrm{T}$, and for all the new PFs, $\breve{\boldsymbol{y}}_n \triangleq \big[\breve{\boldsymbol{y}}_n^{(1)\mathrm{T}} \cdots \breve{\boldsymbol{y}}_n^{(J)\mathrm{T}}\big]^\mathrm{T}$.

A. Association Vectors

For each PA, measurements $\boldsymbol{z}_{m,n}^{(j)}$, are subject to a DA uncertainty. It is not known which measurement $\boldsymbol{z}_{m,n}^{(j)}$ is associated with which PF k, or if a measurement $\boldsymbol{z}_{m,n}^{(j)}$ did not originate from any PF (*false alarm*) or if a PF did not give rise to any measurement (*missed detection*). The probability that a PF is "detected", in the sense that it generates a measurement $\boldsymbol{z}_{m,n}^{(j)}$ in the MPC parameter estimation stage, is denoted by $P_\mathrm{d}(\boldsymbol{x}_n, \underline{\boldsymbol{y}}_{k,n}^{(j)}) \triangleq P_\mathrm{d}(u_{k,n}^{(j)})$, being defined by its normalized amplitude $u_{k,n}^{(j)}$. The distribution of false alarm measurements $f_\mathrm{FA}(\boldsymbol{z}_{m,n}^{(j)})$ is assumed to be known and is defined in (III-D). The associations between measurements $\boldsymbol{z}_{m,n}^{(j)}$ and the PFs at time n can be described by the K-dimensional feature-oriented DA vector $\boldsymbol{c}_n^{(j)} = [c_{1,n}^{(j)} \cdots c_{K,n}^{(j)}]^\mathrm{T}$, with entries $c_{k,n}^{(j)} = m \in \mathcal{M}_n^{(j)}$, if PF k generates $\boldsymbol{z}_{m,n}^{(j)}$ and 0, if PF k does not generate any $\boldsymbol{z}_{m,n}^{(j)}$. In addition, we consider the M_n-dimensional measurement-oriented DA vector $\boldsymbol{b}_n^{(j)} = [b_{1,n}^{(j)} \cdots b_{M_n,n}^{(j)}]^\mathrm{T}$ with entries $b_{m,n}^{(j)} = k \in \mathcal{K}_n^{(j)}$, if $\boldsymbol{z}_{m,n}^{(j)}$ is generated by PF k and 0 is not generated by any PF [20], [23].

B. State Evolution

The agent state $\boldsymbol{x}_n$ and the augmented states of the legacy PFs, $\tilde{\boldsymbol{y}}_{k,n}^{(j)}$, are assumed to evolve independently according to Markovian state dynamics, i.e.,

$$f\big(\boldsymbol{x}_n, \tilde{\boldsymbol{y}}_n | \boldsymbol{x}_{n-1}, \boldsymbol{y}_{n-1}\big) = f(\boldsymbol{x}_n|\boldsymbol{x}_{n-1}) \times \prod_{j=1}^{J} \prod_{k=1}^{K_{n-1}^{(j)}} f(\tilde{\boldsymbol{y}}_{k,n}^{(j)} | \boldsymbol{y}_{k,n-1}^{(j)}), \quad (2)$$

where $f(\boldsymbol{x}_n|\boldsymbol{x}_{n-1})$ and $f(\tilde{\boldsymbol{y}}_{k,n}^{(j)}|\boldsymbol{y}_{k,n-1}^{(j)})$ are the state-transition pdfs of the agent and of legacy PF (j,k), respectively. Note that $\tilde{\boldsymbol{y}}_{k,n}^{(j)}$ depends on both $\tilde{\boldsymbol{y}}_{k,n-1}^{(j)}$ and $\breve{\boldsymbol{y}}_{m,n-1}^{(j)}$. If PF (j,k) existed at time $n-1$, i.e., $r_{k,n-1}^{(j)} = 1$, it either dies, i.e., $\tilde{r}_{k,n}^{(j)} = 0$, or survives, i.e., $\tilde{r}_{k,n}^{(j)} = 1$; in the latter case, it becomes/remains a legacy PF at time n. The probability of survival is denoted by P_s. If the PF survives, its new state $\underline{\tilde{\boldsymbol{y}}}_{k,n}^{(j)}$ is distributed according to the state-transition pdf $f\big(\underline{\tilde{\boldsymbol{y}}}_{k,n}^{(j)} | \underline{\boldsymbol{y}}_{k,n-1}^{(j)}\big)$ (for details cf. [6]).

C. Prior Distribution of Feature- and Measurement-oriented Association Variables

The number of false alarms is assumed Poisson distributed with mean $\mu_\mathrm{FA}^{(j)}$ [26]. The false alarm probability P_FA is discussed in Section III-D. Similarly, the number of newly detected features is assumed Poisson distributed with mean $\mu_{\mathrm{n},n}^{(j)}$; the calculation of $\mu_{\mathrm{n},n}^{(j)}$ will be discussed in Section IV. The joint conditional prior probability mass function of $\boldsymbol{c}_n^{(j)}$ and $\boldsymbol{b}_n^{(j)}$, $\breve{\boldsymbol{r}}_n^{(j)}$, and the number of measurements/new PFs, $M_n^{(j)}$, given the legacy PF's states $\tilde{\boldsymbol{u}}_n^{(j)} \triangleq [\tilde{u}_{1,n}^{(j)\mathrm{T}} \cdots \tilde{u}_{k,n}^{(j)\mathrm{T}}]^\mathrm{T}$ and $\tilde{\boldsymbol{r}}_n^{(j)}$, can be expressed as [6], [17], [20]

$$\begin{aligned} p(\boldsymbol{c}_n^{(j)}, \boldsymbol{b}_n^{(j)}, \breve{\boldsymbol{r}}_n^{(j)}, M_n^{(j)} | \boldsymbol{u}_n^{(j)}, \tilde{\boldsymbol{r}}_n^{(j)}) \\ \propto \psi\big(\boldsymbol{c}_n^{(j)}, \boldsymbol{b}_n^{(j)}\big) \left(\prod_{m=1}^{M_n^{(j)}} h_1\big(\breve{r}_{m,n}^{(j)}, b_{m,n}^{(j)}; K_n^{(j)}\big) \right) \\ \times \left(\prod_{k=1}^{K^{(j)}} g_1\big(\tilde{u}_{k,n}^{(j)}, \tilde{r}_{k,n}^{(j)}, c_{k,n}^{(j)}; M_n^{(j)}\big) \right). \end{aligned} \quad (3)$$

The exclusion indicator function

$$\psi\big(\boldsymbol{c}_n^{(j)}, \boldsymbol{b}_n^{(j)}\big) \triangleq \prod_{k=1}^{K_n^{(j)}} \prod_{m=1}^{M_n^{(j)}} \psi\big(c_{k,n}^{(j)}, b_{m,n}^{(j)}\big), \quad (4)$$

where $\psi\big(c_{k,n}^{(j)}, b_{m,n}^{(j)}\big)$ is defined to be 0 if either $c_{k,n}^{(j)} = m$ and $b_{m,n}^{(j)} \neq k$ or $b_{m,n}^{(j)} = k$ and $c_{k,n}^{(j)} \neq m$, and 1 otherwise. The indicator function enforces that the kth PF can generate at most one measurement, or vice versa, a measurement originates from at most one PF. The factors $h_1\big(\breve{\boldsymbol{r}}_{m,n}^{(j)}, b_{m,n}^{(j)}; K_n^{(j)}\big)$ and $g_1\big(\tilde{u}_{k,n}^{(j)}, \tilde{\boldsymbol{r}}_{k,n}^{(j)}, c_{k,n}^{(j)}; M_n^{(j)}\big)$ are respectively given by

$$h_1\big(1, b_{m,n}^{(j)}; K_n^{(j)}\big) \triangleq \begin{cases} 0, & b_{m,n}^{(j)} \in \mathcal{K}_n^{(j)} \\ \dfrac{\mu_{\mathrm{n},n}^{(j)}}{\mu_\mathrm{FA}^{(j)}}, & b_{m,n}^{(j)} = 0 \end{cases} \quad (5)$$

and $h_1\big(0, b_{m,n}^{(j)}; K_n^{(j)}\big) \triangleq f_\mathrm{D}\big(\breve{\boldsymbol{a}}_{m,n}^{(j)}\big)$ and $g_1\big(\tilde{u}_{k,n}^{(j)}, 1, c_{k,n}^{(j)}; M_n^{(j)}\big) = P_\mathrm{d}\big(u_{k,n}^{(j)}\big)/\mu_\mathrm{FA}^{(j)}$, if $c_{k,n}^{(j)} \in \mathcal{M}_n^{(j)}$ and $1 - P_\mathrm{d}\big(u_{k,n}^{(j)}\big)$, if $c_{k,n}^{(j)} = 0$, and $g_1\big(\tilde{u}_{k,n}^{(j)}, 0, c_{k,n}^{(j)}; M_n^{(j)}\big) \triangleq 1\big(c_{k,n}^{(j)}\big)$, where the indicator function is $1(c) = 1$ if $c = 0$ and 0 otherwise.

The states of newly detected features are assumed to be a priori independent and identically distributed (iid) according to some pdf $f_{\mathrm{n},n}\big(\underline{\boldsymbol{y}}_{m,n}^{(j)}\big)$, whose calculation will be discussed in Section IV. The prior pdf of the states of new PFs for PA j, $\breve{\underline{\boldsymbol{y}}}_n^{(j)}$, conditioned on $\breve{\boldsymbol{r}}_n^{(j)}$ and $M_n^{(j)}$ is then obtained as

$$f\big(\breve{\underline{\boldsymbol{y}}}_n^{(j)} \big| \breve{\boldsymbol{r}}_n^{(j)}, M_n^{(j)}\big) = \left(\prod_{m \in \mathcal{N}_{\breve{\boldsymbol{r}}_n^{(j)}}} f_{\mathrm{n},n}\big(\underline{\breve{\boldsymbol{y}}}_{m,n}^{(j)}\big) \right) \prod_{m' \in \bar{\mathcal{N}}_{\breve{\boldsymbol{r}}_n^{(j)}}} f_\mathrm{D}\big(\underline{\breve{\boldsymbol{y}}}_{m',n}^{(j)}\big),$$

where $\bar{\mathcal{N}}_{\breve{\boldsymbol{r}}_n^{(j)}} \triangleq \mathcal{M}_n^{(j)} \setminus \mathcal{N}_{\breve{\boldsymbol{r}}_n^{(j)}}$ and $\mathcal{N}_{\breve{\boldsymbol{r}}_n^{(j)}} \triangleq \big\{m \in \mathcal{M}_n^{(j)} : \breve{r}_{m,n}^{(j)} = 1\big\}$. Note that before the measurements are obtained, $M_n^{(j)}$ and, thus, the length of the vectors $\breve{\boldsymbol{a}}_n^{(j)}$ and $\breve{\boldsymbol{r}}_n^{(j)}$ is random. In Section IV, a way to introduce prior information on new PFs will be discussed.

D. Likelihood Function

Let us consider $f\big(\boldsymbol{z}_n^{(j)} \big| \boldsymbol{x}_n, \tilde{\boldsymbol{y}}_n^{(j)}, \breve{\boldsymbol{y}}_n^{(j)}, \boldsymbol{c}_n^{(j)}, M_n^{(j)}\big)$ as a *likelihood function*, i.e., a function of $\boldsymbol{x}_n$, $\tilde{\boldsymbol{y}}_n^{(j)}$, $\breve{\boldsymbol{y}}_n^{(j)}$, $\boldsymbol{c}_n^{(j)}$, and $M_n^{(j)}$, for observed $\boldsymbol{z}_n^{(j)}$. If $\boldsymbol{z}_n^{(j)}$ is observed and therefore fixed, also $M_n^{(j)}$ is fixed, and we can write [6], [20]

$$\begin{aligned} f\big(\boldsymbol{z}_n^{(j)} \big| \boldsymbol{x}_n, \tilde{\boldsymbol{y}}_n^{(j)}, \breve{\boldsymbol{y}}_n^{(j)}, \boldsymbol{c}_n^{(j)}, M_n^{(j)}\big) \propto \prod_{m \in \mathcal{N}_{\breve{\boldsymbol{r}}_n^{(j)}}} \frac{f\big(\boldsymbol{z}_{m,n}^{(j)} \big| \boldsymbol{x}_n, \underline{\breve{\boldsymbol{y}}}_{m,n}^{(j)}\big)}{f_\mathrm{FA}\big(\boldsymbol{z}_{m,n}^{(j)}\big)} \\ \times \left(\prod_{k=1}^{K_n^{(j)}} g_2\big(\boldsymbol{x}_n, \underline{\tilde{\boldsymbol{y}}}_{k,n}^{(j)}, \tilde{r}_{k,n}^{(j)}, c_{k,n}^{(j)}; \boldsymbol{z}_n^{(j)}\big) \right). \end{aligned} \quad (6)$$

Here, the factors $g_2\big(\boldsymbol{x}_n, \underline{\tilde{\boldsymbol{y}}}_{k,n}^{(j)}, \tilde{r}_{k,n}^{(j)}, c_{k,n}^{(j)}; \boldsymbol{z}_n^{(j)}\big)$ are defined as

$$g_2\big(\boldsymbol{x}_n, \underline{\tilde{\boldsymbol{y}}}_{k,n}^{(j)}, 1, c_{k,n}^{(j)}; \boldsymbol{z}_n^{(j)}\big) \triangleq \begin{cases} \dfrac{f\big(\boldsymbol{z}_{m,n}^{(j)} \big| \boldsymbol{x}_n, \underline{\tilde{\boldsymbol{y}}}_{k,n}^{(j)}\big)}{f_\mathrm{FA}\big(\boldsymbol{z}_{m,n}^{(j)}\big)}, & c_{k,n}^{(j)} = m \\ 1, & c_{k,n}^{(j)} = 0 \end{cases}$$

and $g_2\big(\boldsymbol{x}_n, \underline{\tilde{\boldsymbol{y}}}_{k,n}^{(j)}, 0, c_{k,n}^{(j)}; \boldsymbol{z}_n^{(j)}\big) \triangleq 1$. We assume that the conditional pdfs of MPC measurements factorize as $f(\boldsymbol{z}_{m,n}^{(j)} | \boldsymbol{x}_n, \underline{\boldsymbol{y}}_{k,n}^{(j)}) = f(\hat{d}_{m,n}^{(j)}, \hat{\varphi}_{m,n}^{(j)} | \boldsymbol{x}_n, \underline{\boldsymbol{y}}_{k,n}^{(j)}) f(\hat{u}_{m,n}^{(j)} | u_{k,n}^{(j)})$, and the false alarm measurements as $f_\mathrm{FA}(\boldsymbol{z}_{m,n}^{(j)}) = f_\mathrm{FA}(\hat{d}_{m,n}^{(j)})$ $f_\mathrm{FA}(\hat{\varphi}_{m,n}^{(j)}) f_\mathrm{FA}(\hat{u}_{m,n}^{(j)})$. The pdf $f(\hat{d}_{m,n}^{(j)}, \hat{\varphi}_{m,n}^{(j)} | \boldsymbol{x}_n, \underline{\boldsymbol{y}}_{k,n}^{(j)})$ of the MPC distance $d_{m,n}^{(j)}$ and angle $\varphi_{m,n}^{(j)}$ conditioned on the agent state $\boldsymbol{x}_n$ and the feature state $\underline{\boldsymbol{y}}_{k,n}^{(j)}$ factors to the pdfs

$$f(\hat{d}_{m,n}^{(j)} | \boldsymbol{x}_n, \underline{\boldsymbol{y}}_{k,n}^{(j)}) = C_1 \mathrm{e}^{-\frac{\left(\hat{d}_{m,n}^{(j)} - \|\boldsymbol{p}_n - \boldsymbol{a}_{k,n}^{(j)}\|\right)^2}{2\hat{\sigma}_{d,m,n}^{(j)\,2}}} \quad (7)$$

$$f(\hat{\varphi}_{m,n}^{(j)} | \boldsymbol{x}_n, \underline{\boldsymbol{y}}_{k,n}^{(j)}) = C_2 \mathrm{e}^{-\frac{\left(\hat{\varphi}_{m,n}^{(j)} - (\angle(\boldsymbol{a}_{k,n}^{(j)} - \boldsymbol{p}_n) - \psi_n)\right)^2}{2\hat{\sigma}_{\varphi,m,n}^{(j)\,2}}}, \quad (8)$$

where $C_1 = (2\pi\hat{\sigma}_{d,m,n}^{(j)\,2})^{-\frac{1}{2}}$ and $C_2 = (2\pi\hat{\sigma}_{\varphi,m,n}^{(j)\,2})^{-\frac{1}{2}}$ with variances $\hat{\sigma}_{d,m,n}^{(j)\,2} = c^2/(8\pi^2\beta^2\hat{u}_{m,n}^{(j)\,2})$ and $\hat{\sigma}_{\varphi,m,n}^{(j)\,2} =$

$c^2/\big(8\pi^2 f_\mathrm{c}^2 \hat{u}_{m,n}^{(j)2} D^2\big(\hat{\varphi}_{m,n}^{(j)}\big)\big)$ with β^2 as the mean square bandwidth of the transmit pulse $s(t)$ and $D^2\big(\hat{\varphi}_{m,n}^{(j)}\big)$ as squared array aperture [21]. The respective false alarm pdfs are assumed to be uniform in the respective domains, i.e., $f_\mathrm{FA}(\hat{d}_{m,n}^{(j)}) = 1/d_\mathrm{max}$ and $f_\mathrm{FA}(\hat{\varphi}_{m,n}^{(j)}) = 1/(2\pi)$.

The pdf of the normalized amplitude $\hat{u}_{m,n}^{(j)}$ conditioned on the PF's amplitude state $u_{k,n}^{(j)}$ is given by a unit-variance Rician distribution [26, Ch. 1.6.6], i.e.,

$$f(\hat{u}_{m,n}|u_{k,n}) = \frac{\hat{u}_{m,n}\mathrm{e}^{(-(\hat{u}_{m,n}^2+u_{k,n}^2)/2)} I_0\big(\hat{u}_{m,n}u_{k,n}\big)}{P_\mathrm{d}(u_{k,n})}, \quad (9)$$

where $I_0(\cdot)$ is the 0th order modified first-kind Bessel function. The detection probability related to the Rician model is given as $P_\mathrm{d}(u_{k,n}) = Q_1(u_{k,n}, \sqrt{2\ln(1/P_\mathrm{FA})})$, where $Q_1(\cdot,\cdot)$ is the Marcum Q-function [26, Ch. 1.6.6]. The false alarm pdf of the normalized amplitude $\hat{u}_{m,n}$ is given by a unit-variance Rayleigh distribution [26, Ch. 1.6.6], i.e., $f_\mathrm{FA}(\hat{u}_{m,n}) = \hat{u}_{m,n}\exp(-\hat{u}_{m,n}^2/2)/P_\mathrm{FA}$. Hence, the false alarm probability is given as $P_\mathrm{FA} = \exp(-u_\mathrm{th}^2/2)$ with threshold u_th.

E. Joint Posterior pdf

Using Bayes' rule and independence assumptions related to the state-transition pdfs (see Section III-B), the prior pdfs (see Section III-C), and the likelihood model (see Section III-D), the joint posterior pdf of $\boldsymbol{x}_{1:n}$ ($\boldsymbol{x}_{1:n} \triangleq [\boldsymbol{x}_1^\mathrm{T}\cdots\boldsymbol{x}_n^\mathrm{T}]^\mathrm{T}$), $\boldsymbol{y}_{1:n}$, $\boldsymbol{c}_{1:n}$, and $\boldsymbol{b}_{1:n}$ given $\boldsymbol{z}_{1:n}$ for all time steps $n' = 1,\ldots,n$

$$\begin{aligned} &f(\boldsymbol{x}_{1:n}, \boldsymbol{y}_{1:n}, \boldsymbol{c}_{1:n}, \boldsymbol{b}_{1:n}, \boldsymbol{m}_{1:n}|\boldsymbol{z}_{1:n}) \quad (10)\\ &\propto f(\boldsymbol{x}_1)\left(\prod_{j'=1}^{J}\prod_{m'=1}^{M_1^{(j')}} h\big(\boldsymbol{x}_1, \breve{\boldsymbol{a}}_{m',1}^{(j')}, \breve{r}_{m',1}^{(j')}, b_{m',1}^{(j')}; \boldsymbol{z}_1^{(j')}\big)\right)\\ &\quad\times\prod_{n'=2}^{n} f(\boldsymbol{x}_{n'}|\boldsymbol{x}_{n'-1})\prod_{j=1}^{J}\psi\big(\boldsymbol{c}_{n'}^{(j)}, \boldsymbol{b}_{n'}^{(j)}\big)\\ &\quad\times\left(\prod_{m=1}^{M_{n'}^{(j)}} h\big(\boldsymbol{x}_{n'}, \underline{\breve{\boldsymbol{y}}}_{m,n'}^{(j)}, \breve{r}_{m,n'}^{(j)}, b_{m,n'}^{(j)}; \boldsymbol{z}_{n'}^{(j)}\big)\right)\\ &\quad\times\prod_{k=1}^{K_{n'-1}^{(j)}} f\big(\tilde{\boldsymbol{y}}_{k,n'}^{(j)}|\boldsymbol{y}_{k,n'-1}^{(j)}\big) g\big(\boldsymbol{x}_{n'}, \underline{\tilde{\boldsymbol{y}}}_{k,n'}^{(j)}, \tilde{r}_{k,n'}^{(j)}, c_{k,n'}^{(j)}; \boldsymbol{z}_{n'}^{(j)}\big), \end{aligned}$$

where $g\big(\cdot,\cdot,\cdot,\cdot;\boldsymbol{z}_n^{(j)}\big) = g_1\big(\cdot,\cdot,\cdot;M_n^{(j)}\big)g_2\big(\cdot,\cdot,\cdot,\cdot;\boldsymbol{z}_n^{(j)}\big)$ and $h\big(\cdot,\cdot,\cdot,\cdot;\boldsymbol{z}_n^{(j)}\big) = h_1\big(\cdot,\cdot;K_n^{(j)}\big)h_2\big(\cdot,\cdot,\cdot,\cdot;\boldsymbol{z}_n^{(j)}\big)$ and

$$\begin{aligned} &h_2\big(\boldsymbol{x}_n, \underline{\breve{\boldsymbol{y}}}_n^{(j)}, 1, b_{m,n}^{(j)}; \boldsymbol{z}_n^{(j)}\big)\\ &\triangleq\begin{cases} 0, & b_{m,n}^{(j)} \in \mathcal{K}_n^{(j)}\\ \dfrac{f_{\mathrm{n},n}\big(\underline{\breve{\boldsymbol{y}}}_{m,n}^{(j)}\big) f\big(\boldsymbol{z}_{m,n}^{(j)}|\boldsymbol{x}_n, \underline{\breve{\boldsymbol{y}}}_{m,n}^{(j)}\big)}{f_\mathrm{FA}\big(\boldsymbol{z}_{m,n}^{(j)}\big)}, & b_{m,n}^{(j)} = 0 \end{cases} \quad (11) \end{aligned}$$

and $h_2\big(\boldsymbol{x}_n, \underline{\breve{\boldsymbol{y}}}_{m,n}^{(j)}, 0, b_{m,n}^{(j)}; \boldsymbol{z}_n^{(j)}\big) \triangleq f_\mathrm{D}\big(\breve{\boldsymbol{a}}_{m,n}^{(j)}\big)$. This factorization of the joint posterior pdf is represented by the factor graph shown in Fig. 2 [27], where subgraphs corresponding to individual PAs are indicated by boxes with light magenta background color. All the factor nodes, variable nodes, and messages related to the agent state are represented in red boldface style, those related to the legacy PF states are represented by the blue parts contained in dashed boxes, those related to the new PF states are represented by the magenta parts contained in dotted boxes, and those related to loopy BP DA are represented by the green parts contained in dashed-dotted boxes. Details about the messages can be found in [6].

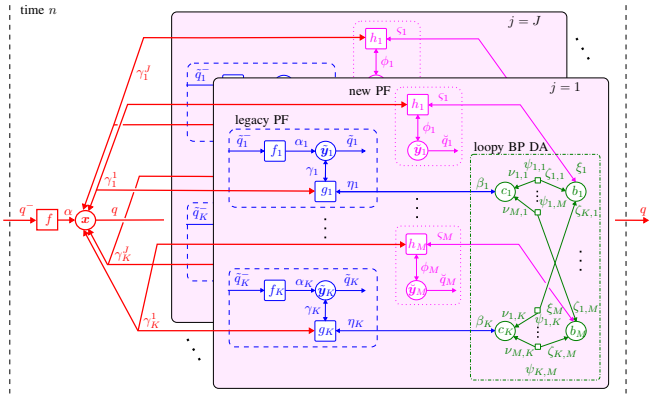

Fig. 2. Factor graph (adapted from [6]) representing the factorization of the joint posterior pdf in (10). Details about the messages can be found in [6].

F. Minimum Mean-Square Error (MMSE) Estimation

Our goal is to estimate the agent state $\boldsymbol{x}_n$ and the positions $\boldsymbol{a}_{k,n}$ and the amplitudes $u_{k,n}$ of the PFs from past and present measurements, i.e., from the total measurement vector $\boldsymbol{z}_{1:n}$. In the Bayesian framework, estimation of the states are based on their respective posterior pdfs. We develop an approximate calculation of the minimum mean-square error (MMSE) estimates of the agent state $\boldsymbol{x}_n$, the positions $\boldsymbol{a}_{k,n}$ and the amplitudes $u_{k,n}$ of the PFs based on the marginal posterior pdfs:

$$\hat{\boldsymbol{x}}_n^\mathrm{MMSE} \triangleq \int \boldsymbol{x}_n f(\boldsymbol{x}_n|\boldsymbol{z}_{1:n})\,\mathrm{d}\boldsymbol{x}_n, \quad (12)$$

$$\hat{\boldsymbol{a}}_{k,n}^{(j)\mathrm{MMSE}} \triangleq \int \boldsymbol{a}_{k,n}^{(j)} f\big(\underline{\boldsymbol{y}}_{k,n}^{(j)}\big|r_{k,n}^{(j)}=1, \boldsymbol{z}_{1:n}\big)\,\mathrm{d}\underline{\boldsymbol{y}}_{k,n}^{(j)}, \quad (13)$$

$$\hat{u}_{k,n}^{(j)\mathrm{MMSE}} \triangleq \int u_{k,n}^{(j)} f\big(\underline{\boldsymbol{y}}_{k,n}^{(j)}\big|r_{k,n}^{(j)}=1, \boldsymbol{z}_{1:n}\big)\,\mathrm{d}\underline{\boldsymbol{y}}_{k,n}^{(j)}, \quad (14)$$

where $f\big(\underline{\boldsymbol{y}}_{k,n}^{(j)}\big|r_{k,n}^{(j)}=1,\boldsymbol{z}_{1:n}\big) = f\big(\underline{\boldsymbol{y}}_{k,n}^{(j)}, r_{k,n}^{(j)}=1\big|\boldsymbol{z}_{1:n}\big)/p\big(r_{k,n}^{(j)}=1\big|\boldsymbol{z}_{1:n}\big)$, and $p\big(r_{k,n}^{(j)}=1\big|\boldsymbol{z}_{1:n}\big) = \int f\big(\underline{\boldsymbol{y}}_{k,n}^{(j)}, r_{k,n}^{(j)}=1\big|\boldsymbol{z}_{1:n}\big)\,\mathrm{d}\underline{\boldsymbol{y}}_{k,n}^{(j)}$. The state of the k-th PF is only estimated if it is considered as detected at time n, i.e., $p\big(r_{k,n}^{(j)}=1\big|\boldsymbol{z}_{1:n}\big) > P_\mathrm{det}$ with detection probability threshold P_det.

G. BP Message Passing Algorithm

The pdfs $f(\boldsymbol{x}_n|\boldsymbol{z}_{1:n})$ and $f\big(\underline{\boldsymbol{y}}_{k,n}^{(j)}, r_{k,n}^{(j)}|\boldsymbol{z}_{1:n}\big)$ in (12), (13), and (14) are marginal pdfs of the joint posterior pdf in (10). Since direct marginalization is infeasible, the marginal pdfs are approximated by means of an efficient BP sum-product message passing algorithm [27] to the factor graph in Fig. 2. All messages shown in Fig. 2 and the according BP algorithm are described in [6, Section V-B]. The following scheduling is introduced for calculating the messages: (i) Message passing is only done forward in time, (ii) iterative message passing is

executed for DA [23] and, (iii) iterative message passing is only executed once to consider the loops involving the agent state and the features. More details can be found in [6].

Once all messages are available (BP algorithm cf. [6, Section V-B]), the beliefs approximating the desired marginal posterior pdfs are obtained. The belief for the agent state is given, up to a normalization factor, by $q(\boldsymbol{x}_n) \propto \alpha(\boldsymbol{x}_n) \prod_{j=1}^{J} \prod_{k \in \mathcal{K}_{n-1}^{(j)}} \gamma_k^{(j)}(\boldsymbol{x}_n)$. This belief (after normalization) provides an approximation of the marginal posterior pdf $f(\boldsymbol{x}_n|\boldsymbol{z}_{1:n})$, and it is used instead of $f(\boldsymbol{x}_n|\boldsymbol{z}_{1:n})$ in (12). Furthermore, the beliefs $\tilde{q}\big(\underline{\tilde{\boldsymbol{y}}}_{k,n}^{(j)}, \tilde{r}_{k,n}^{(j)}\big)$ for the augmented states of the legacy PFs, $\underline{\tilde{\boldsymbol{y}}}_{k,n}^{(j)}$, are calculated as $\tilde{q}\big(\underline{\tilde{\boldsymbol{y}}}_{k,n}^{(j)}, 1\big) \propto \alpha_k\big(\underline{\tilde{\boldsymbol{y}}}_{k,n}^{(j)}, 1\big)\gamma\big(\underline{\tilde{\boldsymbol{y}}}_{k,n}^{(j)}, 1\big)$ and $\tilde{q}\big(\underline{\tilde{\boldsymbol{y}}}_{k,n}^{(j)}, 0\big) \propto \alpha_{k,n}^{(j)}\gamma_{k,n}^{(j)}$. The beliefs $\breve{q}\big(\underline{\breve{\boldsymbol{y}}}_{m,n}^{(j)}, \breve{r}_{m,n}^{(j)}\big)$ for the augmented states of the new PFs, $\underline{\breve{\boldsymbol{y}}}_{m,n}^{(j)}$ are $\breve{q}\big(\underline{\breve{\boldsymbol{y}}}_{m,n}^{(j)}, 1\big) \propto \phi\big(\underline{\breve{\boldsymbol{y}}}_{m,n}^{(j)}, 1\big)$ and $\breve{q}\big(\underline{\breve{\boldsymbol{y}}}_{m,n}^{(j)}, 0\big) \propto \phi_{m,n}^{(j)}$. In particular, $\tilde{q}\big(\underline{\tilde{\boldsymbol{y}}}_{k,n}^{(j)}, 1\big)$ and $\breve{q}\big(\underline{\breve{\boldsymbol{y}}}_{m,n}^{(j)}, 1\big)$ approximate the marginal posterior pdf $f\big(\underline{\boldsymbol{y}}_{k',n}^{(j)}, r_{k',n}^{(j)} = 1 \big| \boldsymbol{z}_{1:n}\big)$, where $k' \in \mathcal{K}_{n-1}^{(j)} \cup \mathcal{M}_n^{(j)}$ (assuming an appropriate index mapping between k and m on the one hand and k' on the other), and they are used in (12)–(14). A computationally feasible approximate calculation of the various messages and beliefs can be based on the sequential Monte Carlo (particle-based) implementation approach introduced in [6], [12], [20].

IV. State Propagation for Undetected Features

In parallel to, and in support of, the BP-based detection and estimation algorithm, we use a "zero-measurement" PHD filter in order to propagate information about features that potentially exist but did not generate any measurement yet. Such features will be termed *undetected features* in what follows. A similar strategy was previously introduced in the context of MTT [22], [23]. This propagation of information about undetected features enables the calculation of the intensity function of newly detected features, $\lambda_n^{\mathrm{n}}\big(\underline{\boldsymbol{y}}_{\cdot,n}^{(j)}\big) = \mu_{\mathrm{n},n}^{(j)} f_{\mathrm{n},n}\big(\underline{\boldsymbol{y}}_{\cdot,n}^{(j)}\big)$, for all PAs j at time n, where $\underline{\boldsymbol{y}}_{\cdot,n}^{(j)}$ denotes a generic single-feature state. Note that $\lambda_n^{\mathrm{n}}\big(\underline{\breve{\boldsymbol{y}}}_{m,n}^{(j)}\big)$ occurs in $h\big(\boldsymbol{x}_n, \underline{\breve{\boldsymbol{y}}}_{m,n}^{(j)}, 1, 0; \boldsymbol{z}_n^{(j)}\big)$ in (11). An extension of this Section and a review of the concept of a Poisson random finite set (RFS), which underlies the PHD filter, can be found in [6].

The original PHD filter [28] propagates the intensity functions of both the detected and undetected features. In [22], [23], a PHD filter is introduced that propagates only the intensity function of the undetected features. In this filter, which we will term a zero-measurement PHD filter, the propagated RFS remains within the class of Poisson RFSs without any approximation. In the proposed SLAM algorithm, the zero-measurement PHD filter complements the BP-based algorithm in Section III-G because it propagates information about undetected features whereas the BP-based algorithm propagates information about detected features. We assume that at the initial time $n=1$, the state of the undetected features for PA j is a Poisson RFS with intensity function $\lambda_n^{\mathrm{u}}\big(\underline{\boldsymbol{y}}_{\cdot,1}^{(j)}\big)$. If no prior information on the spatial distribution of VAs and PAs is incorporated, $\lambda_n^{\mathrm{u}}\big(\underline{\boldsymbol{y}}_{\cdot,1}^{(j)}\big)$ is constant on the region of interest (ROI), with the integral of $\lambda_n^{\mathrm{u}}\big(\underline{\boldsymbol{y}}_{\cdot,1}^{(j)}\big)$ over the ROI chosen equal to the expected number of features in the ROI. Using a zero-measurement PHD filter, state propagation for the undetected features amounts to propagating the intensity function of the Poisson RFS (i.e., $\lambda_n^{\mathrm{u}}\big(\underline{\boldsymbol{y}}_{\cdot,n-1}^{(j)}\big) \rightarrow \lambda_n^{\mathrm{u}}\big(\underline{\boldsymbol{y}}_{\cdot,n}^{(j)}\big)$).

1) Prediction Step: In the prediction step, which is identical to that of the original PHD filter [28], the preceding intensity function $\lambda_{n-1}^{\mathrm{u}}\big(\underline{\boldsymbol{y}}_{\cdot,n-1}^{(j)}\big)$ is converted into a "predicted intensity function" $\lambda_{n|n-1}^{\mathrm{u}}\big(\underline{\boldsymbol{y}}_{\cdot,n}^{(j)}\big)$ according to

$$\lambda_{n|n-1}^{\mathrm{u}}\big(\underline{\boldsymbol{y}}_{\cdot,n}^{(j)}\big) = P_{\mathrm{s}} \int f\big(\underline{\boldsymbol{y}}_{\cdot,n}^{(j)} \big| \underline{\boldsymbol{y}}_{\cdot,n-1}^{(j)}\big)\, \lambda_{n-1}^{\mathrm{u}}\big(\underline{\boldsymbol{y}}_{\cdot,n-1}^{(j)}\big)\, \mathrm{d}\underline{\boldsymbol{y}}_{\cdot,n-1}^{(j)} + \lambda^{\mathrm{b}}\big(\underline{\boldsymbol{y}}_{\cdot,n}^{(j)}\big), \tag{15}$$

where $f\big(\underline{\boldsymbol{y}}_{\cdot,n}^{(j)} \big| \underline{\boldsymbol{y}}_{\cdot,n-1}^{(j)}\big)$ is the state-transition pdf of the undetected feature state. Furthermore, $\lambda^{\mathrm{b}}\big(\underline{\boldsymbol{y}}_{\cdot,n}^{(j)}\big)$ is the intensity function of a Poisson RFS that models the birth of new features. From $\lambda_{n|n-1}^{\mathrm{u}}\big(\underline{\boldsymbol{y}}_{\cdot,n}^{(j)}\big)$, the pdf $f_{\mathrm{n},n}\big(\underline{\boldsymbol{y}}_{\cdot,n}^{(j)}\big)$ for newly detected features for PA j is obtained as [22]

$$f_{\mathrm{n},n}\big(\underline{\boldsymbol{y}}_{\cdot,n}^{(j)}\big) = \frac{P_{\mathrm{d}}^{(j)}\big(u_{\cdot,n}^{(j)}\big)\, \lambda_{n|n-1}^{\mathrm{u}}\big(\underline{\boldsymbol{y}}_{\cdot,n}^{(j)}\big)}{\int P_{\mathrm{d}}^{(j)}\big(u_{\cdot,n}^{(j)}\big)\, \lambda_{n|n-1}^{\mathrm{u}}\big(\underline{\boldsymbol{y}}_{\cdot,n}^{(j)\prime}\big) \mathrm{d}\underline{\boldsymbol{y}}_{\cdot,n}^{(j)\prime}}, \tag{16}$$

where $P_{\mathrm{d}}^{(j)}\big(u_{\cdot,n}^{(j)}\big)$ is the detection probability of the undetected feature state for PA j. Furthermore, the mean number of newly detected features is given by $\mu_{\mathrm{n},n}^{(j)} = \int\int P_{\mathrm{d}}^{(j)}\big(u_{\cdot,n}^{(j)}\big) \times \lambda_{n|n-1}^{\mathrm{u}}\big(\underline{\boldsymbol{y}}_{\cdot,n}^{(j)}\big) \alpha(\boldsymbol{x}_n)\, \mathrm{d}\underline{\boldsymbol{y}}_{\cdot,n}^{(j)}\, \mathrm{d}\boldsymbol{x}_n$ ($\alpha(\boldsymbol{x}_n)$ is provided by the BP algorithm cf. [6, Section V-B]). As mentioned earlier, $f_{\mathrm{n},n}\big(\underline{\boldsymbol{y}}_{\cdot,n}^{(j)}\big)$ and $\mu_{\mathrm{n},n}^{(j)}$ are needed in (5) and (11).

2) Update Step: In the update step, the predicted intensity function $\lambda_{n|n-1}^{\mathrm{u}}\big(\underline{\boldsymbol{y}}_{\cdot,n}^{(j)}\big)$ is converted into the new (updated) intensity function $\lambda_n^{\mathrm{u}}\big(\underline{\boldsymbol{y}}_{\cdot,n}^{(j)}\big)$ according to [22], [23]

$$\lambda_n^{\mathrm{u}}\big(\underline{\boldsymbol{y}}_{\cdot,n}^{(j)}\big) = \big(1 - P_{\mathrm{d}}^{(j)}\big(u_{\cdot,n}^{(j)}\big)\big)\, \lambda_{n|n-1}^{\mathrm{u}}\big(\underline{\boldsymbol{y}}_{\cdot,n}^{(j)}\big). \tag{17}$$

We note that this update relation is identical to that of the original PHD filter [28] for the case where no measurements are available. The intensity function $\lambda_n^{\mathrm{u}}\big(\underline{\boldsymbol{y}}_{\cdot,n}^{(j)}\big)$ represents essentially "negative information" in the sense that for $\lambda^{\mathrm{b}}\big(\underline{\boldsymbol{y}}_{\cdot,n}^{(j)}\big) = 0$, $\lambda_n^{\mathrm{u}}\big(\underline{\boldsymbol{y}}_{\cdot,n}^{(j)}\big)$ is high in those parts of the ROI that have not been explored by the mobile agent yet, and for $\lambda^{\mathrm{b}}\big(\underline{\boldsymbol{y}}_{\cdot,n}^{(j)}\big) > 0$, it is high in those parts of the ROI that have not been explored for some time. The expressions (15) and (17) are calculated by using a sequential Monte Carlo implementation, similarly to [29].

V. Performance Evaluation

a) Synthetic Data: We apply the algorithm to synthetically generated data, modeling a seminar room at Graz University of Technology [6, Fig. 1]. The true MPC parameters, distance, AoA, and amplitude are calculated for the set of PAs and VAs as in [6, Fig. 1], with 6 and 5 features for PA 1 and PA 2 respectively (including the PA positions). The amplitudes follow the free-space pathloss and are attentuated

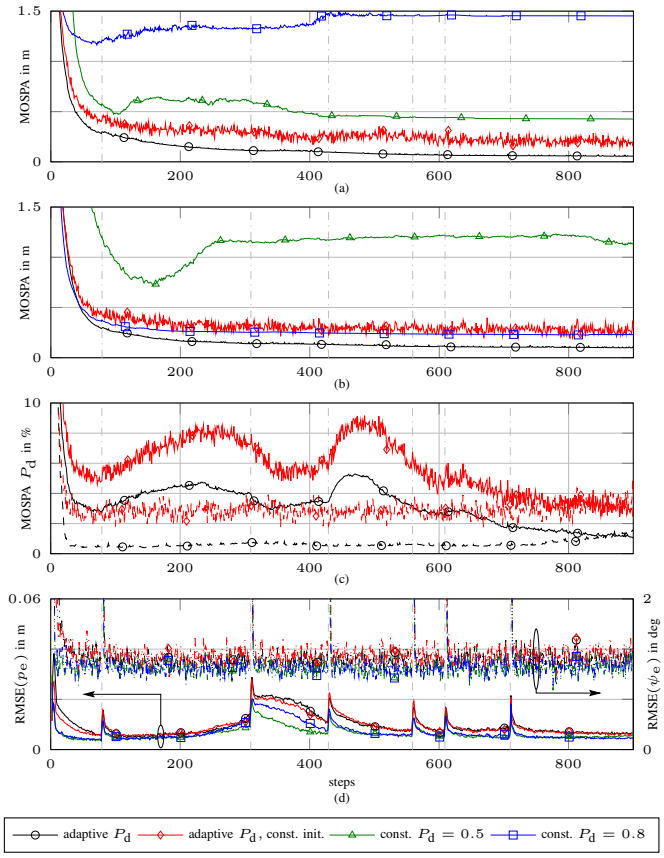

Fig. 3. MOSPA error on the PF positions for PA 1 (a) and PA 2 (b). (c): RMSE of the agent position (solid) and orientation (dashed). MOSPA error on the detection probabilities of the PFs (d) for PA 1 (solid) and PA 2 (dashed), respectively.

by 3 dB for reflected MPCs. The DM is simulated with a delay power spectrum according to [30] with signal-to-interference-ratio SIR $= 10\log_{10}(\sum_l |\alpha_l|^2/\Omega) = 7$ dB where Ω is the total DM power. Furthermore, the signal-to-noise-ratio SNR $= 10\log_{10}(\sum_l |\alpha_l|^2/N_0) = 30$ dB. To synthesize the delay and angular variances given in Sec. III-D, the following signal is used: a root-raised-cosine filter with symbol period $T_{\mathrm{p}} = 0.8\,\mathrm{ns}$ and roll-off factor of 0.6 at $f_{\mathrm{c}} = 7\,\mathrm{GHz}$, leading to an absolute bandwidth of 2 GHz. Furthermore, a quadratic 3×3 array with an inter-element spacing of 1 cm is simulated. In each simulation run we generated with detection probability $P_{\mathrm{d}}(u_{l,n}^{(j)}) = Q_1(u_{l,n}^{(j)}, 2\ln(1/P_{\mathrm{FA}}))$ the noisy measurements according to (7), (8), and (9) using the true MPC parameters. The P_{FA} is calculated for a threshold of $u_{\mathrm{th}} = 1.95$ (cf. Sec. III-D). In addition to the true noisy measurements we generate a mean number of $\mu_{\mathrm{FA}}^{(j)} = 1$ false alarm measurements after thresholding for both PA 1 and PA 2 according to the pdfs given in Sec. III-D with $d_{\max} = 30\,\mathrm{m}$.

The birth intensity function $\lambda^{\mathrm{b}}(\underline{\boldsymbol{y}}_{\cdot,n}^{(j)})$ is uniform on the ROI, which is a circular disk of radius 30 m around the center of the floor plan [6, Fig. 1]. Thus, $\lambda^{\mathrm{b}}(\underline{\boldsymbol{y}}_{\cdot,n}^{(j)}) = \mu_{\mathrm{b}}/(2\pi(30\,\mathrm{m})^2)$. Similarly, the initial undetected feature intensity is uniform on the ROI, i.e., $\lambda_1^{\mathrm{u}}(\underline{\boldsymbol{y}}_{\cdot,1}^{(j)}) = \mu_{\mathrm{n},1}^{(j)}/(2\pi(30\,\mathrm{m})^2)$. We compare the zero-measurement PHD filter to the case were the number of undetected and therefore undetected feature intensity is constant along time $\lambda_1^{\mathrm{u}}(\underline{\boldsymbol{y}}_{\cdot,1}^{(j)}) = 0.1/(2\pi(30\,\mathrm{m})^2)$.

The following other parameters are used: the number of particles is 30.000, $P_{\mathrm{s}} = 0.999$, $\mu_{\mathrm{b}} = 10^{-4}$, $\mu_{\mathrm{n},1} = 6$, the detection probability threshold $P_{\mathrm{det}} = 0.5$, the pruning threshold $P_{\mathrm{prun}} = 10^{-3}$ (cf. [6, Sec. V-A]), the $P_{\mathrm{d}}(\hat{u}_{k,n}^{\mathrm{MMSE}})$ is determined by the MMSE estimate of the amplitudes $u_{k,n}$. The state-transition pdf of the amplitudes $f(u_{k,n}|u_{k,n-1})$ is chosen as Gaussian distribution with variance $\sigma_{\mathrm{u},k,n} = 0.05\hat{u}_{k,n}^{\mathrm{MMSE}}/s$. The agents' state-transition pdf is defined by a linear, near constant-turn motion model [1, Chapter 5] with $\Delta T = 1\,\mathrm{s}$, longitudinal velocity noise $\sigma_{\mathrm{v,l}} = 0.01\,\mathrm{m/s}$, and rotational velocity noise $\sigma_{\mathrm{v,r}} = 0.52\,\mathrm{rad/s}$. The particles for the initial agent state are drawn from a 4-D uniform distribution with center $\boldsymbol{x}_1 = [\boldsymbol{p}_1^{\mathrm{T}}\ 0\ 0]^{\mathrm{T}}$ and with the position uniform within $[-5, 5]\,\mathrm{m}$, and longitudinal and rotational velocity uniform within $[-0.03, 0.03]\,\mathrm{m/s}$ and $[-0.52, 0.52]\,\mathrm{rad/s}$, respectively. We perform 100 simulation runs.

The mean optimal subpattern assignment (MOSPA) error [31] on the PF positions, including PAs and VAs, is shown in Fig. 3a and Fig. 3b for PA 1 and PA 2, respectively. As can clearly be seen, the MOSPA error on the PF positions are worse, if AI is not utilized in the algorithm (const. P_{d}), since the algorithm cannot detect "weak" features with a low detection probability. Fig. 3d shows the MOSPA error for the adaptive detection probability for PA 1 and PA 2 in solid and dashed lines respectively. If the initialization parameters of new PFs are constant, i.e. the undetected feature intensity is constant, and set to a larger value than the birth intensity, clutter measurements are detected more often and thus the MOSPA error of the PF positions and P_{d} are increased (More experimental investigations can be found in [24].). The agents' root mean square position error $\mathrm{RMSE}(p_{\mathrm{e}})$ is depicted in Fig. 3d with solid lines (left y axis) and is below 2 cm for the entire trajectory. The RMSE of the agents' orientation error $\mathrm{RMSE}(\psi_{\mathrm{e}})$ is represented by dash-dotted lines in Fig. 3d (right y axis) and is below 2°. Both, the RMSE on the position and the orientation do not strongly depend on the employed algorithm. Interestingly, the agent state errors are larger although the MOSPA error is smaller. This counter-intuitive fact is explained by the much larger variance of the posterior pdfs of "weak" features, which are simply discarded by the algorithm using a constant detection probability.

b) Measured Data: Finally, we apply the algorithm to data measured in a seminar room at Graz University of Technology [6]. The data is measured with a correlative channel sounder with 7 GHz bandwidth centered at 6.95 GHz. Then, the bandwidth is reduced to 2 GHz with the previously introduced signal and AWGN is added such that SNR $= 35$ dB. To estimate the MPC parameters, we utilize the previously introduced (Sec. II) sparse Bayesian multipath channel estimator [25].[1] Compared to the synthetic setup, we changed the mean

[1] As the utilized virtual antenna array was not well calibrated (positioned by hand), we employ a Rayleigh model (strongly fluctuating target with dominant scattering center) for (9) instead of the Rician model [26, Ch. 1.6.7 and 4.6.2].

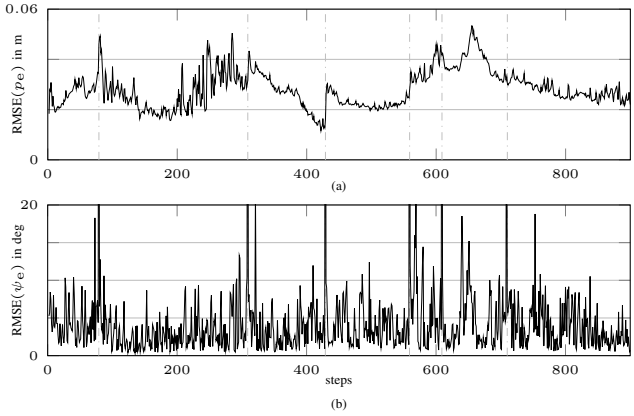

Fig. 4. RMSE of the agent position (a) and orientation (b).

number of birth to $\mu_{\mathrm{b}} = 10^{-3}$ and the mean number of false alarm measurements to $\mu_{\mathrm{FA}}^{(j)} = 3$.

Fig. 4a and Fig. 4b show the RMSEs of the agents' position and orientation obtained for the trajectory over time, respectively. The agent's position and orientation RMSEs over time are mostly below $4\,\mathrm{cm}$ and $10\,^\circ$, respectively.

VI. Conclusions

We have extended a radio-signal-based SLAM algorithm with probabilistic DA that uses amplitude information of MPCs to exploit also the estimated AoAs of the MPCs acquired from an antenna array at the mobile agent. Furthermore, we propose a "zero-measurement" PHD filter for initializing new PFs and compare its performance to constant initialization parameters of new PFs over time. The use of AoA information allows to estimate the agent orientation jointly with the agent position with high accuracy. The PHD filter improves the initialization of new features into the state space.

References

[1] S. Thrun, W. Burgard, and D. Fox, *Probabilistic Robotics (Intelligent Robotics and Autonomous Agents)*. Cambridge, MA, USA: MIT Press, 2005.

[2] G. Bresson, Z. Alsayed, L. Yu, and S. Glaser, "Simultaneous localization and mapping: A survey of current trends in autonomous driving," *IEEE Trans. Intell. Veh.*, vol. 2, no. 3, pp. 194–220, Sept. 2017.

[3] J. Levinson, J. Askeland, J. Becker, J. Dolson, D. Held, S. Kammel, J. Z. Kolter, D. Langer, O. Pink, V. Pratt, M. Sokolsky, G. Stanek, D. Stavens, A. Teichman, M. Werling, and S. Thrun, "Towards fully autonomous driving: Systems and algorithms," in *n Proc. IEEE IV-11*, Baden-Baden, Germany, Jun. 2011, pp. 163–168.

[4] R. Di Taranto, S. Muppirisetty, R. Raulefs, D. Slock, T. Svensson, and H. Wymeersch, "Location-aware communications for 5G networks: How location information can improve scalability, latency, and robustness of 5G," *IEEE Signal Process. Mag.*, vol. 31, no. 6, pp. 102–112, Nov. 2014.

[5] C. Gentner, T. Jost, W. Wang, S. Zhang, A. Dammann, and U. C. Fiebig, "Multipath assisted positioning with simultaneous localization and mapping," *IEEE Trans. Wireless Commun.*, vol. 15, no. 9, pp. 6104–6117, Sep. 2016.

[6] E. Leitinger, F. Meyer, F. Hlawatsch, K. Witrisal, F. Tufvesson, and M. Z. Win, "A belief propagation algorithm for multipath-based SLAM," *Corr*, vol. arXiv:1801.04463v3, 2018.

[7] E. Leitinger, P. Meissner, C. Rudisser, G. Dumphart, and K. Witrisal, "Evaluation of position-related information in multipath components for indoor positioning," *IEEE J. Sel. Areas Commun.*, vol. 33, no. 11, pp. 2313–2328, Nov. 2015.

[8] R. Mendrzik, H. Wymeersch, G. Bauch, and Z. Abu-Shaban, "Harnessing NLOS components for position and orientation estimation in 5G millimeter wave MIMO," vol. 18, no. 1, pp. 93–107, Jan. 2019.

[9] A. Shahmansoori, G. E. Garcia, G. Destino, G. Seco-Granados, and H. Wymeersch, "Position and orientation estimation through millimeter-wave MIMO in 5G systems," *IEEE Trans. Wireless Commun.*, vol. 17, no. 3, pp. 1822–1835, Mar. 2018.

[10] H. Wymeersch, N. Garcia, H. Kim, G. Seco-Granados, S. Kim, F. Went, and M. Fröhle, "5G mm wave downlink vehicular positioning," in *Proc. IEEE GLOBECOM-18*, Dec. 2018, pp. 206–212.

[11] H. Wymeersch, J. Lien, and M. Win, "Cooperative localization in wireless networks," *Proc. IEEE*, vol. 97, no. 2, pp. 427 –450, Feb. 2009.

[12] F. Meyer, O. Hlinka, H. Wymeersch, E. Riegler, and F. Hlawatsch, "Distributed localization and tracking of mobile networks including noncooperative objects," *IEEE Trans. Signal Inf. Process. Netw.*, vol. 2, no. 1, pp. 57–71, Mar. 2016.

[13] F. Meyer, B. Etzlinger, Z. Liu, F. Hlawatsch, and M. Z. Win, "A scalable algorithm for network localization and synchronization," *IEEE Internet Things J.*, vol. 5, no. 6, pp. 4714–4727, Dec. 2018.

[14] M. Z. Win, F. Meyer, Z. Liu, W. Dai, S. Bartoletti, and A. Conti, "Efficient multisensor localization for the internet of things: Exploring a new class of scalable localization algorithms," *IEEE Signal Process. Mag.*, vol. 35, no. 5, pp. 153–167, Sept 2018.

[15] F. Meyer and M. Z. Win, "Joint navigation and multitarget tracking in networks," in *Proc. IEEE ICC-18*, May 2018, pp. 1–6.

[16] F. Meyer, Z. Liu, and M. Z. Win, "Network localization and navigation using measurements with uncertain origin," in *Proc. Fusion-18*, July 2018, pp. 1–7.

[17] E. Leitinger, S. Grebien, X. Li, F. Tufvesson, and K. Witrisal, "On the use of MPC amplitude information in radio signal based SLAM," in *Proc. IEEE SSP-18*, Freiburg, Germany, June 2018, pp. 633–637.

[18] E. Leitinger, F. Meyer, F. Tufvesson, and K. Witrisal, "Factor graph based simultaneous localization and mapping using multipath channel information," in *Proc. IEEE ICC-17*, Paris, France, Jun. 2017.

[19] D. Lerro and Y. Bar-Shalom, "Automated tracking with target amplitude information," in *1990 American Control Conference*, May 1990, pp. 2875–2880.

[20] F. Meyer, T. Kropfreiter, J. L. Williams, R. Lau, F. Hlawatsch, P. Braca, and M. Z. Win, "Message passing algorithms for scalable multitarget tracking," *Proc. IEEE*, vol. 106, no. 2, pp. 221–259, Feb. 2018.

[21] T. Wilding, S. Grebien, E. Leitinger, U. Mühlmann, and K. Witrisal, "Single-anchor, multipath-assisted indoor positioning with aliased antenna arrays," in *Proc. Asilomar-18*, Pacifc Grove, CA, USA, Oct. 2018, pp. 525–531.

[22] P. Horridge and S. Maskell, "Using a probabilistic hypothesis density filter to confirm tracks in a multi-target environment," July 2011.

[23] J. L. Williams, "Marginal multi-Bernoulli filters: RFS derivation of MHT, JIPDA, and association-based MeMBer," *IEEE Trans. Aerosp. Electron. Syst.*, vol. 51, no. 3, pp. 1664–1687, Jul. 2015.

[24] ——, "Hybrid Poisson and multi-Bernoulli filters," in *Proc. FUSION-12*, Jul. 2012, pp. 1103–1110.

[25] S. Grebien, E. Leitinger, B. H. Fleury, X. Li, D. Shutin, and K. Witrisal, "Super-resolution channel estimation including the dense multipath component — A sparse variational Bayesian approach," in preperation.

[26] Y. Bar-Shalom and X.-R. Li, *Multitarget-Multisensor Tracking: Principles and Techniques*. Storrs, CT, USA: Yaakov Bar-Shalom, 1995.

[27] F. Kschischang, B. Frey, and H.-A. Loeliger, "Factor graphs and the sum-product algorithm," *IEEE Transactions on Information Theory*, vol. 47, no. 2, pp. 498–519, Feb 2001.

[28] R. Mahler, *Statistical Multisource-Multitarget Information Fusion*. Norwood, MA, USA: Artech House, Inc., 2007.

[29] T. Kropfreiter, F. Meyer, and F. Hlawatsch, "Sequential Monte Carlo implementation of the track-oriented marginal multi-Bernoulli/Poisson filter," in *Proc. FUSION-16*, Heidelberg, Germany, Jul. 2016, pp. 972–979.

[30] J. Karedal, S. Wyne, P. Almers, F. Tufvesson, and A. Molisch, "A measurement-based statistical model for industrial ultra-wideband channels," *IEEE Trans. Wireless Commun.*, vol. 6, no. 8, pp. 3028–3037, Aug. 2007.

[31] D. Schuhmacher, B.-T. Vo, and B.-N. Vo, "A consistent metric for performance evaluation of multi-object filters," *IEEE Trans. Signal Process.*, vol. 56, no. 8, pp. 3447–3457, Aug. 2008.